Metal oxidation states in biological water splitting

Vera Krewald [†], *Marius Retegan* [†], *Nicholas Cox* [†], *Johannes Messinger* [‡], *Wolfgang Lubitz* [†], *Serena DeBeer* [†], *Frank Neese* [†], *Dimitrios A. Pantazis* [†]*

† Max Planck Institute for Chemical Energy Conversion, Stiftstr. 34-38, 45470 Mülheim an der Ruhr, Germany.

‡ Department of Chemistry, Chemical Biological Center (KBC), Umeå University, 90187 Umeå, Sweden.

Supporting Information

Contents:

Part I. Additional computational details and results on model complexes

Backbone constraints

Selected backbone atoms were constrained to the coordinates of the 1.9 Å resolution crystallographic model (PDB ID 3ARC, PSII monomer A),[1] in order to ensure that the geometry optimizations of all OEC models remain consistent with the higher-order protein folding conformation, and to provide anchor points for residues that are not part of a continuous peptide chain (such as Tyr161). The constrained atoms are depicted in Figure S1.

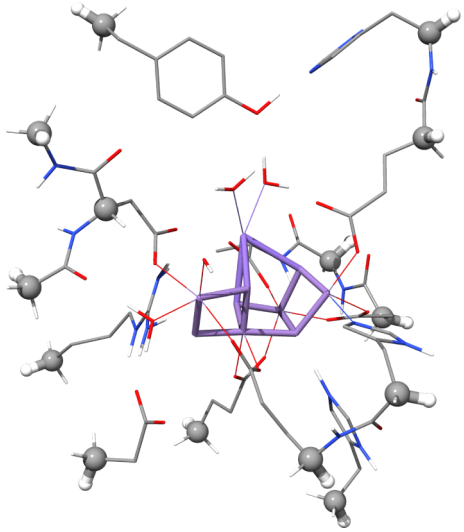

Figure S1. One of the computational models used in this study, with the constrained backbone carbon atoms and connected constrained hydrogen atoms shown as spheres. Non-coordinating waters and many hydrogen atoms have been omitted for clarity.

Prediction of ground state spin multiplicity as a reliable criterion for model evaluation

The present theoretical approach[2-5] consists of using broken-symmetry DFT to obtain the exchange coupling constants J_{ij} by singular value decomposition and then diagonalizing the Heisenberg–Dirac–van Vleck Hamiltonian with these exchange coupling constants in order to obtain the ladder of spin states. Its success in accurately predicting the nature of magnetic coupling in manganese dimers has been amply demonstrated in the literature by various research groups for a large number of systems (see for example [6-10]) and needs not be emphasized again here. The method was so far proven to perform flawlessly for Mn

complexes of higher nuclearity as well.[2, 5, 11] Figures S2 and S3 collect some examples, most of them previously unpublished, of trinuclear and tetranuclear Mn complexes with magnetically interacting Mn ions in various oxidation states and various coordination/bridging geometries. Regardless of the spin topology, the nature of the (super)exchange interactions and the final total spin that is observed experimentally, the current approach always yields the correct ground state multiplicity.

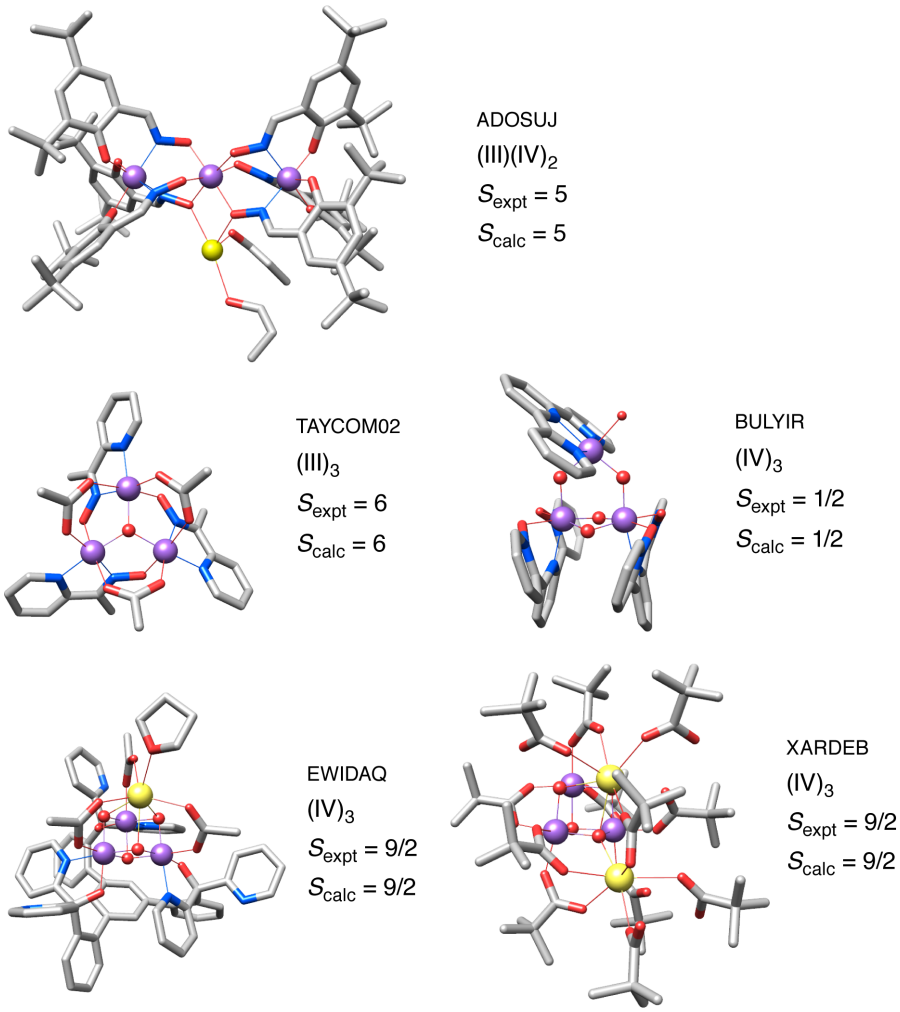

Figure S2. Examples of synthetic exchange-coupled trinuclear Mn complexes.[11-15] For each one, the Cambridge Structural Database (CSD) access code is provided, followed by the Mn oxidation states of the compound, the experimentally determined ground state spin, and the ground state spin computed by the method employed in this work.

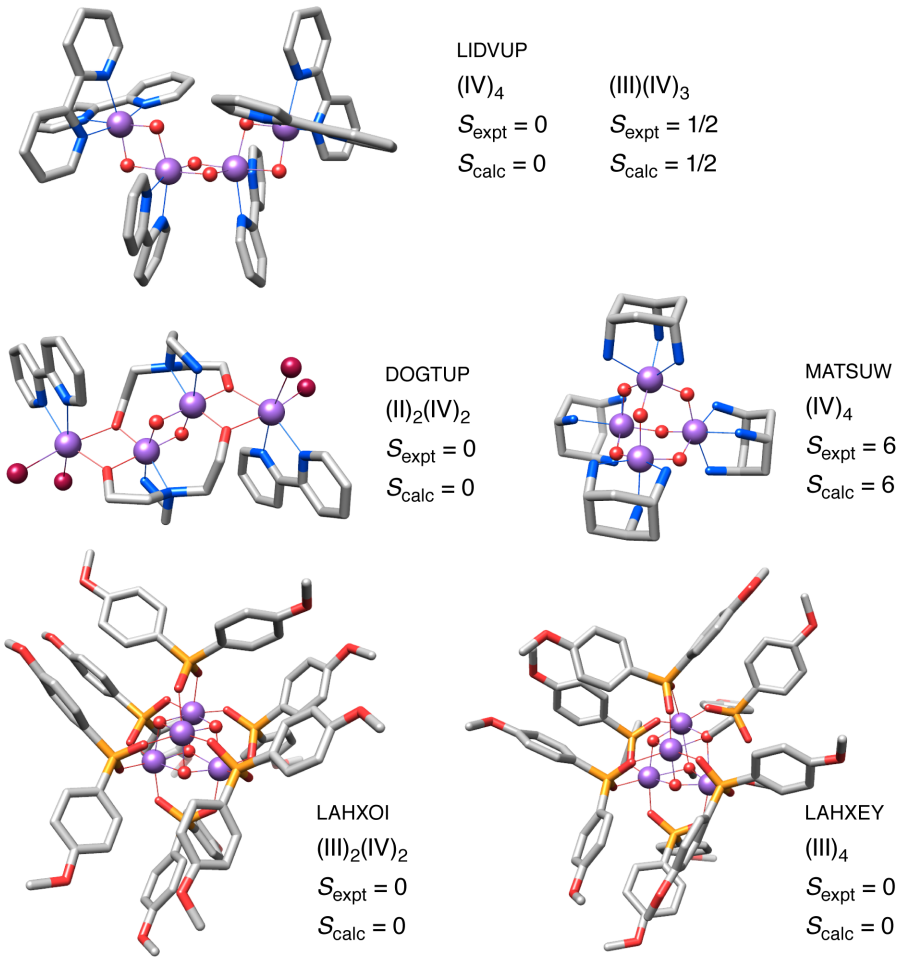

Figure S3. Examples of synthetic exchange-coupled tetranuclear Mn complexes.[16-20] For each one, the CSD access code is provided, followed by the Mn oxidation states of the compound, the experimentally determined ground state spin, and the ground state spin computed by the method employed in this work.

Part II. Schematic diagrams of additional models and 3D core representations

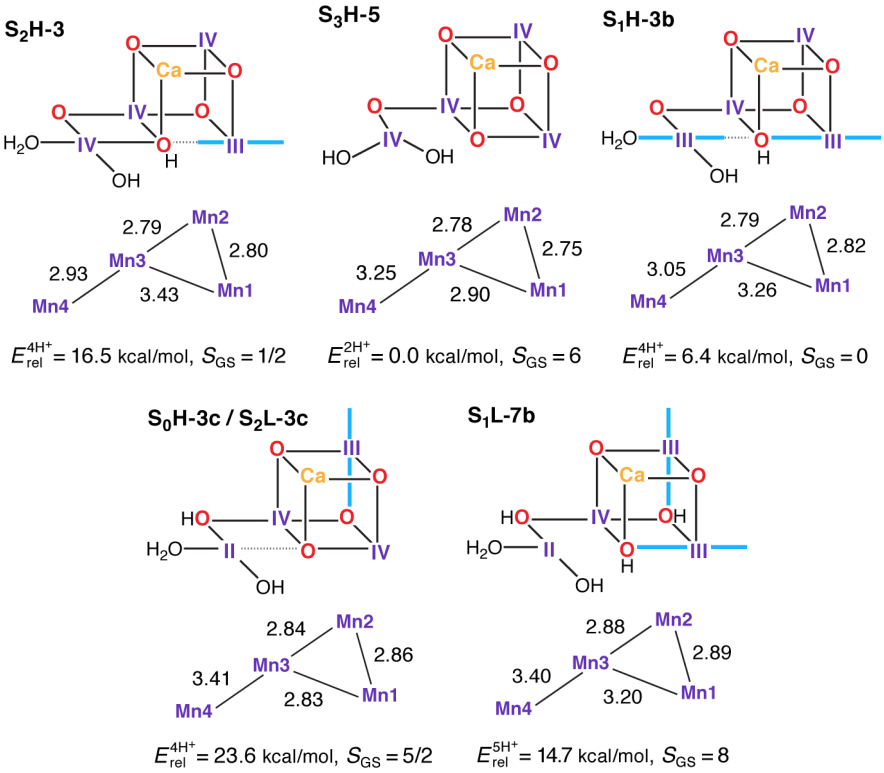

Figure S4. Additional models not shown in the main text.

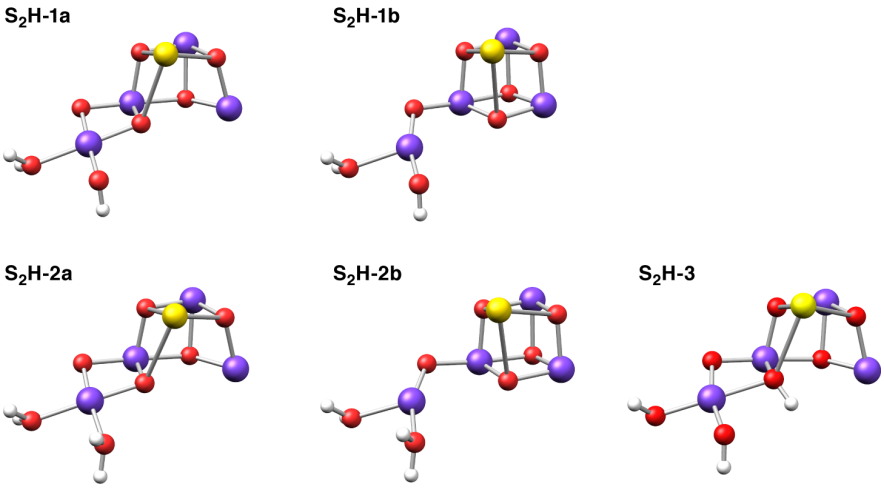

Figure S5. Optimized core geometries for the S_2H models. Color code: Mn purple, Ca yellow, O red, H white.

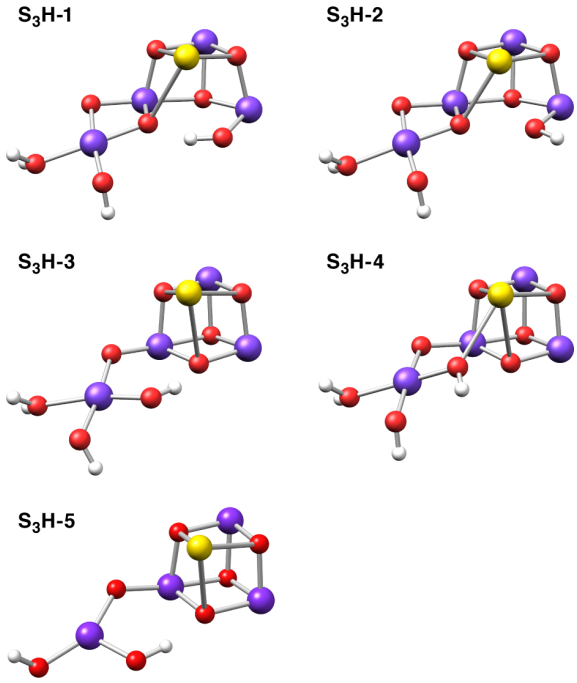

Figure S6. Optimized core geometries for the S_3H models.

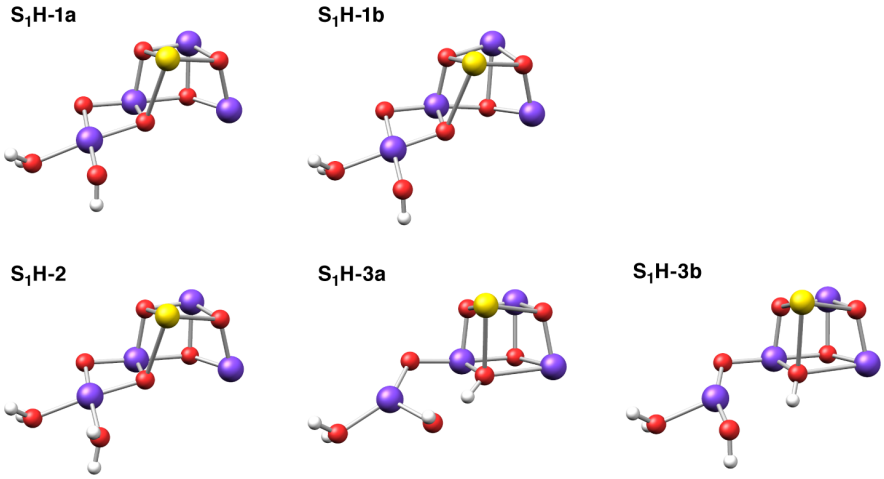

Figure S7. Optimized core geometries for the S_1H models.

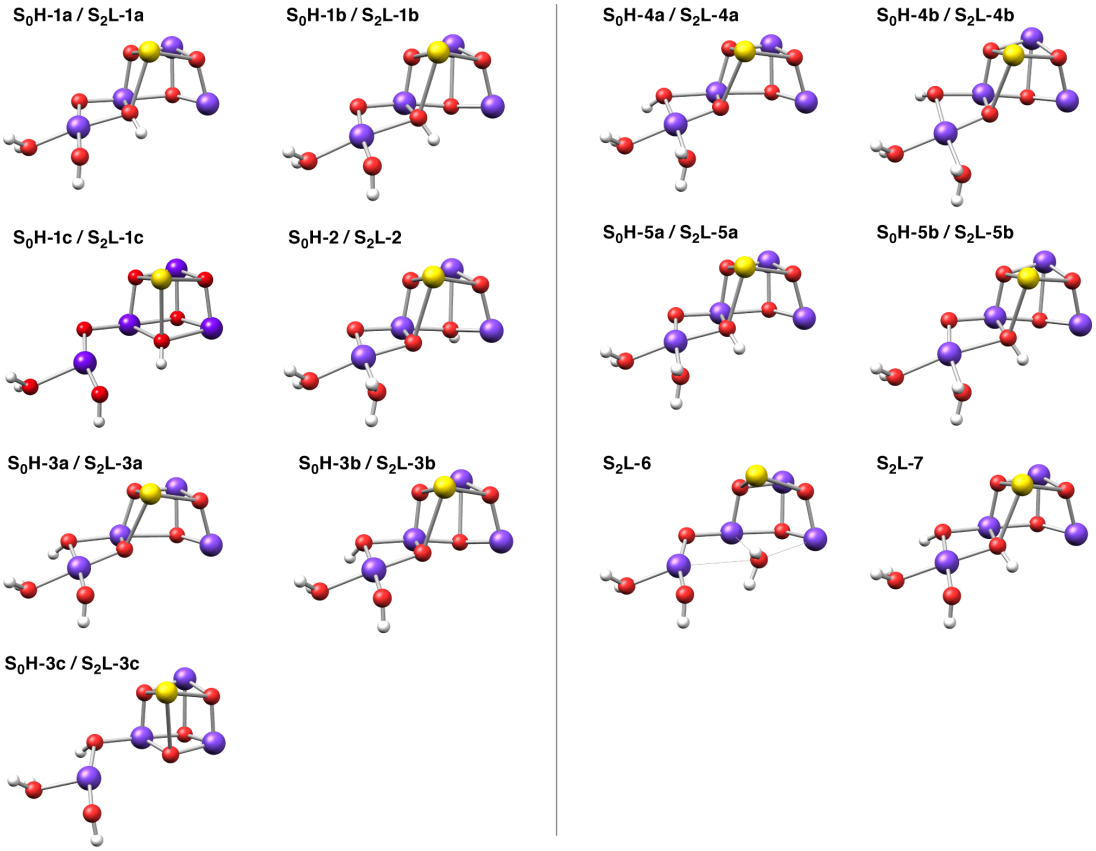

Figure S8. Optimized core geometries for the S_0H and S_2L models.

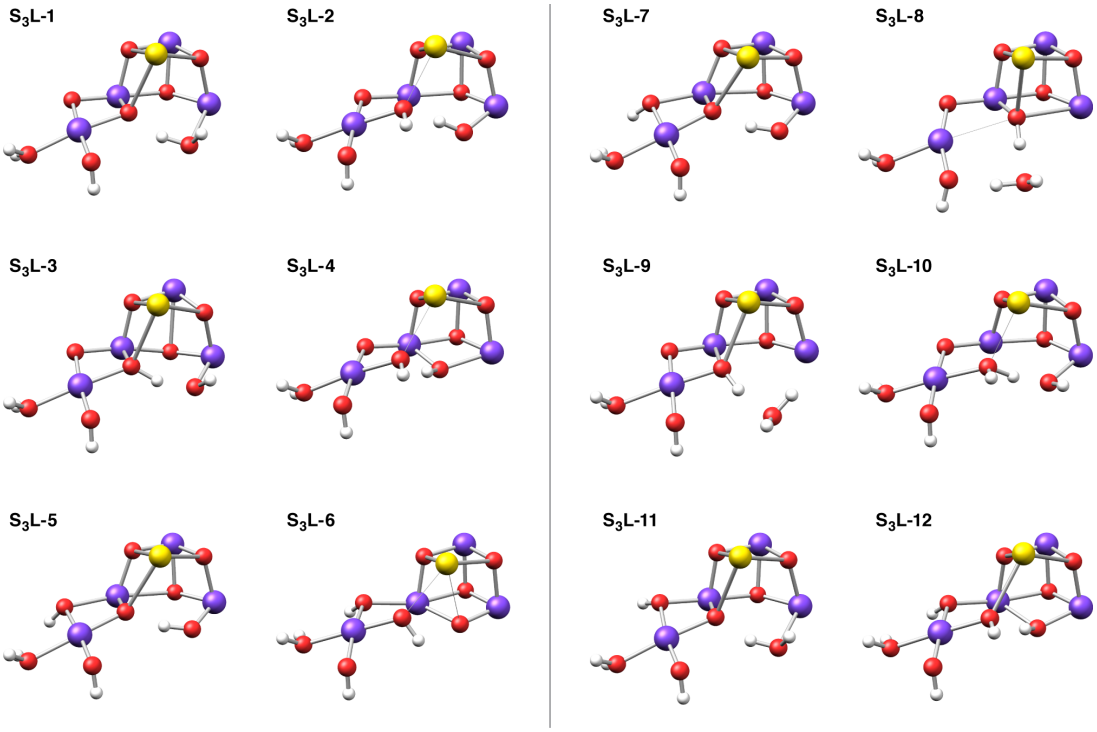

Figure S9. Optimized core geometries for the S_3L models.

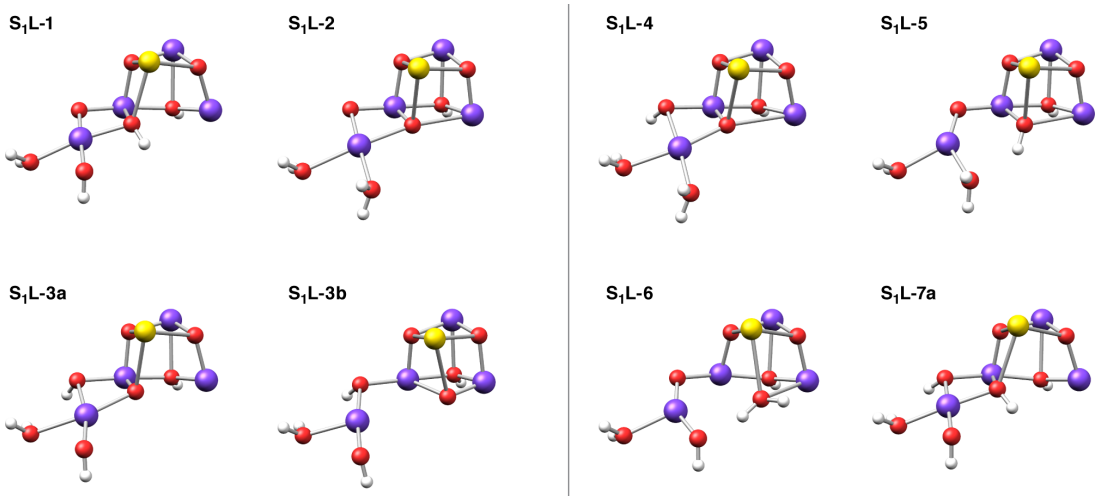

Figure S10. Optimized core geometries for the S_1L models.

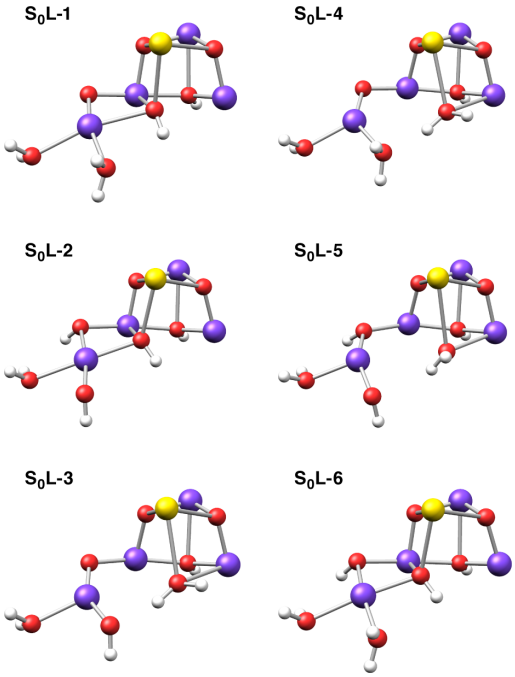

Figure S11. Optimized core geometries for the S_0L models.

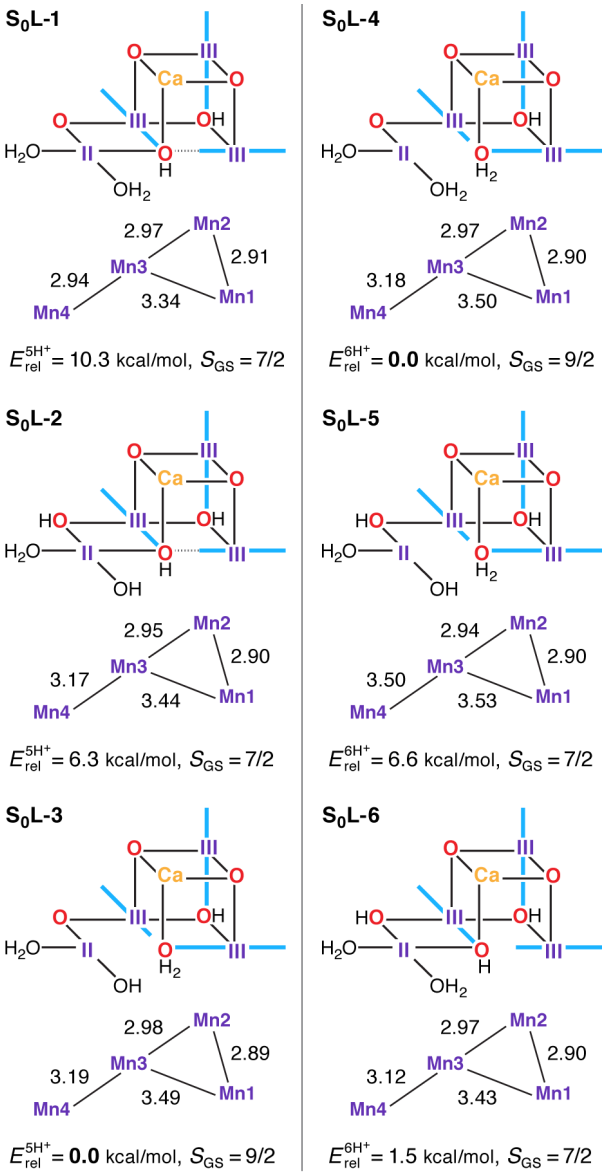

Figure S12. Protonation patterns, oxidation states, relative total energies and ground spin states for the S_0L models. Blue lines indicate the orientation of Jahn–Teller axes.

Part III. Exchange coupling constants and additional spectroscopic properties

Table S1. Exchange coupling constants J (cm^{-1}), ground spin state (S_{GS}), first excited spin state (S_{ES}) and their energy separation ΔE (cm^{-1}) for the S_2H models.

		J_{12}	J_{13}	J_{14}	J_{23}	J_{24}	J_{34}	S_{GS}	S_{ES}	ΔE
3 H^+	**S_2H-1a**	–15.8	1.9	1.2	23.1	1.9	–13.9	1/2	3/2	22.0
	S_2H-1b	30.5	12.9	4.5	36.5	1.3	–7.3	5/2	7/2	0.3
4 H^+	**S_2H-2a**	–15.4	1.5	1.3	23.7	1.7	–13.1	1/2	3/2	21.2
	S_2H-2b	32.6	11.7	4.0	37.3	1.5	–2.6	13/2	11/2	10.5
	S_2H-3	–14.7	–4.6	0.3	17.9	1.7	–13.4	1/2	3/2	24.7

Table S2. Exchange coupling constants J (cm^{-1}), ground spin state (S_{GS}), first excited spin state (S_{ES}) and their energy separation ΔE (cm^{-1}) for the S_3H models.

		J_{12}	J_{13}	J_{14}	J_{23}	J_{24}	J_{34}	S_{GS}	S_{ES}	ΔE
4 H^+	**S_3H-1**	12.4	–5.6	3.9	18.7	0.9	–14.7	3	4	16.3
	S_3H-2	14.1	–5.0	4.8	9.5	1.2	–19.8	3	4	28.1
	S_3H-3	30.0	5.4	2.2	34.8	1.6	–8.4	3	4	9.9
	S_3H-4	29.4	11.4	0.5	33.0	1.9	–8.8	3	4	15.6
	S_3H-5	31.5	9.7	4.8	30.7	2.2	0.9	6	5	30.9

Table S3. Exchange coupling constants J (cm^{-1}), ground spin state (S_{GS}), first excited spin state (S_{ES}) and their energy separation ΔE (cm^{-1}) for the S_1H models.

		J_{12}	J_{13}	J_{14}	J_{23}	J_{24}	J_{34}	S_{GS}	S_{ES}	ΔE
3 H^+	**S_1H-1a**	–15.6	7.7	–6.0	21.0	0.8	–56.9	0	1	16.9
	S_1H-1b	6.1	–3.4	1.7	31.4	–0.3	–10.7	4	3	15.8
4 H^+	**S_1H-2**	–15.2	6.8	–6.0	17.4	1.4	–71.0	0	1	23.1
	S_1H-3a	–21.9	14.2	–1.3	21.9	1.8	–25.5	0	1	23.0
	S_1H-3b	–21.7	10.7	–6.9	19.6	0.7	–9.5	0	1	2.6

Table S4. Exchange coupling constants J (cm^{-1}), ground spin state (S_{GS}), first excited spin state (S_{ES}) and their energy separation ΔE (cm^{-1}) for the S_0H and S_2L models.

		J_{12}	J_{13}	J_{14}	J_{23}	J_{24}	J_{34}	S_{GS}	S_{ES}	ΔE
4 H^+	**S_0H-1a** **S_2L-1a**	–15.5	–5.7	0.0	–35.2	1.1	–0.4	1/2	3/2	1.9
	S_0H-1b **S_2L-1b**	4.5	–7.4	–2.5	32.3	1.1	–2.3	7/2	5/2	1.3
	S_0H-1c **S_2L-1c**	–32.2	4.1	–6.3	–40.1	0.1	–4.0	1/2	3/2	21.3
	S_0H-2 **S_2L-2**	9.1	0.4	1.1	35.6	0.4	–63.4	7/2	5/2	68.8
	S_0H-3a **S_2L-3a**	–18.9	–7.2	–0.2	43.4	–0.2	–5.8	1/2	3/2	15.6
	S_0H-3b **S_2L-3b**	4.1	1.3	0.4	43.6	–0.3	–24.2	7/2	5/2	34.7
	S_0H-3c **S_2L-3c**	49.1	1.0	8.9	48.7	0.7	–20.6	5/2	7/2	3.6
5 H^+	**S_0H-4a** **S_2L-4a**	–19.2	–8.6	0.3	41.5	0.3	1.6	7/2	5/2	11.4
	S_0H-4b **S_2L-4b**	1.7	–3.0	2.3	31.6	0.1	10.5	15/2	13/2	7.5
	S_0H-5a **S_2L-5a**	–15.4	–5.7	0.2	–33.9	1.1	3.9	9/2	7/2	9.7
	S_0H-5b **S_2L-5b**	3.9	–8.7	–4.8	31.2	0.7	10.1	7/2	9/2	20.2
	S_2L-6	–19.9	–8.1	–1.2	–22.0	0.7	–14.8	1/2	3/2	14.9
	S_2L-7	–12.1	–8.6	0.3	–19.6	0.6	2.6	5/2	3/2	1.6

Table S5. Exchange coupling constants J (cm^{-1}), ground spin state (S_{GS}), first excited spin state (S_{ES}) and their energy separation ΔE (cm^{-1}) for the S_3L models.

		J_{12}	J_{13}	J_{14}	J_{23}	J_{24}	J_{34}	S_{GS}	S_{ES}	ΔE
5 H^+	**S_3L-1**	–27.8	1.1	–8.7	6.7	0.3	–56.8	0	1	43.3
	S_3L-2	12.4	2.6	–2.7	–29.5	1.3	–14.4	3	2	7.0
	S_3L-3	20.5	2.3	–0.6	42.5	5.6	–24.1	3	4	30.1
	S_3L-4	–33.0	25.0	–2.1	17.6	0.8	–19.1	0	1	24.7
	S_3L-5	24.8	–28.2	–2.2	44.4	–0.4	–4.1	0	1	0.3
	S_3L-6	37.0	28.6	0.5	3.5	0.1	9.9	7	6	46.4
	S_3L-7	24.9	–23.4	–2.2	44.0	–0.4	–3.7	1	2	7.1
6 H^+	**S_3L-8**	–22.4	11.7	–5.2	22.5	0.4	0.2	3	2	6.2
	S_3L-9	–16.8	–15.2	1.1	–22.7	–10.0	–3.7	2	1	5.8
	S_3L-10	9.4	–4.2	–1.7	–25.3	1.2	–17.2	3	2	35.3
	S_3L-11	–28.2	1.7	–5.7	13.0	–0.3	–35.6	0	1	26.3
	S_3L-12	28.5	27.9	–0.5	–20.8	–0.2	–3.2	1	2	0.1

Table S6. Exchange coupling constants J (cm^{-1}), ground spin state (S_{GS}), first excited spin state (S_{ES}) and their energy separation ΔE (cm^{-1}) for the S_1L models.

		J_{12}	J_{13}	J_{14}	J_{23}	J_{24}	J_{34}	S_{GS}	S_{ES}	ΔE
4 H^+	**S_1L-1**	8.3	–5.3	1.0	3.3	1.3	3.6	6	5	1.6
	S_1L-2	16.5	11.8	–15.3	21.9	–0.2	–31.4	3	4	98.3
	S_1L-3a	11.2	13.7	–5.0	48.0	0.8	–25.8	3	4	59.2
	S_1L-3b	40.7	9.0	–0.9	17.3	2.0	–13.0	3	4	26.1
5 H^+	**S_1L-4**	11.3	12.6	–6.6	35.0	0.1	–34.6	3	4	76.7
	S_1L-5	13.4	6.8	–5.0	21.1	0.1	–49.5	3	4	74.6
	S_1L-6	6.8	–11.3	–2.5	6.2	–2.6	–31.0	3	4	6.3
	S_1L-7a	8.7	–7.4	2.7	24.0	2.9	5.7	8	7	6.1
	S_1L-7b	5.1	10.4	–2.0	46.0	2.7	4.1	8	7	14.4

Table S7. Exchange coupling constants J (cm^{-1}), ground spin state (S_{GS}), first excited spin state (S_{ES}) and their energy separation ΔE (cm^{-1}) for the S_0L models.

		J_{12}	J_{13}	J_{14}	J_{23}	J_{24}	J_{34}	S_{GS}	S_{ES}	ΔE
5 H^+	**S_0L-1**	11.5	–0.4	–6.6	–4.6	–0.1	–26.2	7/2	5/2	36.4
	S_0L-2	9.7	–3.3	–4.6	17.6	–0.3	–2.2	7/2	9/2	19.0
	S_0L-3	9.7	–6.6	0.5	–0.6	–0.5	–36.3	9/2	7/2	36.2
6 H^+	**S_0L-4**	9.8	–7.6	0.0	0.8	–0.4	–39.0	9/2	7.2	29.6
	S_0L-5	10.9	–8.1	–1.0	16.3	–0.3	–10.5	7/2	5/2	11.8
	S_0L-6	7.9	–3.2	–3.6	13.0	–0.2	–3.7	7/2	9/2	21.5

Table S8. Isotropic raw hyperfine coupling constants and their components (ordered according to $|A_1| < |A_2| < |A_3|$) for the **S_3H** and **S_3L** models. A scaling factor of 1.78 was applied.

		A_{iso}	A_1	A_2	A_3
S_3H-1	**Mn1**	-88.5	-80.3	-87.6	-97.7
	Mn2	-85.8	-78.5	-84.2	-94.6
	Mn3	-92.2	-82.5	-90.2	-103.8
	Mn4	123.6	114.5	120.0	136.3
S_3H-2	**Mn1**	-91.6	-83.9	-90.4	-100.4
	Mn2	-99.7	-92.8	-95.6	-110.7
	Mn3	122.3	111.0	121.6	134.4
	Mn4	-125.5	-114.0	-122.1	-140.5
S_3H-3	**Mn1**	-85.5	-81.0	-84.6	-91.1
	Mn2	-84.5	-78.7	-85.9	-88.9
	Mn3	-81.2	-73.7	-77.8	-92.0
	Mn4	119.1	115.0	118.9	123.5
S_3H-4	**Mn1**	-80.4	-73.2	-79.6	-88.6
	Mn2	-85.0	-79.1	-86.8	-89.1
	Mn3	-74.4	-63.1	-74.5	-85.5
	Mn4	116.0	113.9	115.3	118.8
S_3L-2	**Mn1**	-94.0	-87.8	-94.4	-99.8
	Mn2	-98.4	-94.5	-95.6	-105.1
	Mn3	84.8	19.3	114.5	120.5
	Mn4	-92.0	-28.1	-106.5	-141.3
S_3L-3	**Mn1**	-98.0	-93.6	-97.2	-103.3
	Mn2	-113.6	-52.4	-126.9	-161.5
	Mn3	-103.2	-91.9	-101.6	-116.2
	Mn4	136.9	73.8	146.0	190.9
S_3L-8	**Mn1**	96.5	34.1	121.6	133.9
	Mn2	-105.4	-101.5	-103.0	-111.6
	Mn3	-95.1	-88.0	-95.3	-101.9
	Mn4	-113.1	-52.4	-127.0	-159.7
S_3L-10	**Mn1**	-95.3	-92.2	-95.1	-98.7
	Mn2	-96.7	-91.6	-94.3	-104.3
	Mn3	84.6	18.7	114.3	120.8
	Mn4	-115.6	-52.4	-121.6	-172.7

Table S9. Energetic separation ΔE (in cm^{-1}) between the ground state and the lowest energy spin states with spin $S = 0$ and $S = 1$ for the S_1L models. The number n indicates the number of intervening spin states, i.e. which excited state is the state shown.

		ΔE ($S = 0$)	n	ΔE ($S = 1$)	n
4 H^+	**S_1L-1**	21.0	8	19.3	7
	S_1L-2	535.3	14	386.4	7
	S_1L-3a	402.2	12	294.0	7
	S_1L-3b	541.4	30	363.8	16
5 H^+	**S_1L-4**	401.9	9	293.2	5
	S_1L-5	356.8	10	266.6	5
	S_1L-6	37.1	4	28.7	3
	S_1L-7a	167.2	22	152.6	18
	S_1L-7b	299.5	24	231.3	19

Table S10. Energetic separation ΔE (in cm^{-1}) between the ground state and the lowest-energy spin state with $S = 1/2$ for the S_0L models, and the number n of intervening spin states.

		ΔE	n
5 H^+	**S_0L-1**	146.1	10
	S_0L-2	140.7	15
	S_0L-3a	178.5	10
6 H^+	**S_0L-4**	165.5	9
	S_0L-5	65.8	8
	S_0L-6	112.4	12

Part IV. Mn–Mn, Mn–Ca, Mn–O, Ca–O, and Mn–W distances of all models

	S_2H-1a	S_2H-1b	S_2H-2a	S_2H-2b
Mn1-Mn2	2.803	2.752	2.812	2.755
Mn1-Mn3	3.399	2.889	3.400	2.879
Mn1-Mn4	5.066	5.017	5.092	5.046
Mn2-Mn3	2.798	2.765	2.784	2.756
Mn2-Mn4	5.237	5.600	5.207	5.574
Mn3-Mn4	2.756	3.133	2.738	3.116
Mn1-Ca	3.698	3.477	3.698	3.475
Mn2-Ca	3.419	3.478	3.428	3.484
Mn3-Ca	3.562	3.518	3.564	3.512
Mn4-Ca	4.000	4.197	3.983	4.188
Mn1-O1	1.868	1.849	1.869	1.847
Mn1-O3	1.938	1.892	1.951	1.895
Mn1-O5	3.239	1.866	3.277	1.873
Mn2-O1	1.868	1.857	1.866	1.858
Mn2-O2	1.825	1.818	1.835	1.822
Mn2-O3	1.922	1.916	1.933	1.924
Mn3-O2	1.843	1.843	1.830	1.837
Mn3-O3	2.009	1.973	1.973	1.951
Mn3-O4	1.814	1.805	1.850	1.830
Mn3-O5	1.850	1.895	1.858	1.887
Mn4-O4	1.902	1.871	1.824	1.815
Mn4-O5	1.874	3.169	1.862	3.195
Mn4-W1	2.036	2.141	1.999	2.115
Mn4-W2	1.847	1.859	1.989	1.983
Ca-O1	2.495	2.509	2.495	2.511
Ca-O2	2.597	2.586	2.604	2.586
Ca-O5	2.722	2.728	2.712	2.720

	S_3H-1	S_3H-2	S_3H-3	S_3H-4	S_3H-5
Mn1-Mn2	2.805	2.785	2.745	2.749	2.748
Mn1-Mn3	3.525	3.526	2.929	2.913	2.901
Mn1-Mn4	5.278	5.370	5.257	5.213	5.367
Mn2-Mn3	2.822	2.880	2.775	2.767	2.775
Mn2-Mn4	5.322	5.370	5.785	5.637	5.778
Mn3-Mn4	2.806	2.786	3.325	3.222	3.252
Mn1-Ca	3.575	3.480	3.544	3.516	3.494
Mn2-Ca	3.405	3.353	3.503	3.568	3.519
Mn3-Ca	3.624	3.417	3.522	3.457	3.523
Mn4-Ca	4.173	3.999	4.276	3.994	4.487
Mn1-O1	1.881	1.870	1.847	1.852	1.850
Mn1-O3	1.946	1.930	1.901	1.912	1.896
Mn1-O5	3.481	3.587	1.848	1.814	1.874
Mn2-O1	1.829	1.834	1.856	1.848	1.851
Mn2-O2	1.833	1.842	1.812	1.820	1.822
Mn2-O3	1.927	1.920	1.914	1.911	1.920
Mn3-O2	1.834	1.867	1.846	1.846	1.853
Mn3-O3	2.053	2.079	1.993	1.983	1.967
Mn3-O4	1.820	1.820	1.790	1.817	1.805
Mn3-O5	1.859	1.824	1.899	1.885	1.905
Mn4-O4	1.925	1.933	1.936	1.873	1.822
Mn4-O5	1.851	1.825	3.420	3.411	3.538
Mn4-W1	1.991	2.012	2.102	2.020	1.799
Mn4-W2	1.844	1.850	1.891	1.883	1.792
Ca-O1	2.469	2.534	2.562	2.613	2.548
Ca-O2	2.661	2.503	2.581	2.602	2.595
Ca-O5	2.764	2.596	2.762	2.721	2.700

	S_1H-1a	S_1H-1b	S_1H-2	S_1H-3a	S_1H-3b
Mn1-Mn2	2.793	2.863	2.799	2.833	2.815
Mn1-Mn3	3.338	3.342	3.341	3.206	3.255
Mn1-Mn4	5.037	5.071	5.012	5.600	5.297
Mn2-Mn3	2.803	2.937	2.789	2.777	2.789
Mn2-Mn4	5.189	5.376	5.154	5.726	5.554
Mn3-Mn4	2.762	2.762	2.747	3.163	3.053
Mn1-Ca	3.708	3.666	3.716	3.634	3.664
Mn2-Ca	3.416	3.400	3.417	3.453	3.470
Mn3-Ca	3.546	3.522	3.566	3.490	3.590
Mn4-Ca	3.845	4.019	3.835	4.523	4.272
Mn1-O1	1.862	1.854	1.864	1.886	1.880
Mn1-O3	1.916	1.884	1.924	1.968	1.968
Mn1-O5	3.106	3.272	3.120	2.463	2.535
Mn2-O1	1.877	1.889	1.874	1.859	1.854
Mn2-O2	1.798	1.905	1.805	1.824	1.841
Mn2-O3	1.916	2.294	1.924	1.915	1.911
Mn3-O2	1.879	1.823	1.868	1.837	1.828
Mn3-O3	2.020	1.936	1.991	1.970	1.984
Mn3-O4	1.801	1.860	1.824	1.820	1.814
Mn3-O5	1.823	1.867	1.836	1.880	1.951
Mn4-O4	1.906	1.873	1.863	1.844	1.883
Mn4-O5	1.969	1.844	1.928	3.213	2.820
Mn4-W1	2.069	2.069	2.061	2.037	2.129
Mn4-W2	1.881	1.882	2.019	2.019	1.862
Ca-O1	2.508	2.480	2.505	2.552	2.549
Ca-O2	2.607	2.495	2.608	2.586	2.611
Ca-O5	2.600	2.756	2.626	2.564	2.597

	S_0H-1a S_2L-1a	S_0H-1b S_2L-1b	S_0H-1c S_2L-1c	S_0H-2 S_2L-2	S_0H-3a S_2L-3a	S_0H-3b S_2L-3b	S_0H-3c S_2L-3c
Mn1-Mn2	2.789	2.869	2.794	2.904	2.763	2.895	2.857
Mn1-Mn3	3.372	3.339	3.174	3.386	3.610	3.277	2.834
Mn1-Mn4	5.192	5.241	5.058	5.062	5.297	5.096	5.125
Mn2-Mn3	2.810	2.898	2.806	2.955	2.902	2.901	2.842
Mn2-Mn4	5.288	5.449	5.488	5.288	5.366	5.354	5.824
Mn3-Mn4	2.961	2.931	3.032	2.741	2.859	2.865	3.412
Mn1-Ca	3.778	3.732	3.451	3.720	3.787	3.710	3.498
Mn2-Ca	3.435	3.392	3.413	3.395	3.396	3.382	3.410
Mn3-Ca	3.723	3.587	3.588	3.532	3.529	3.524	3.553
Mn4-Ca	3.948	4.075	4.150	3.831	3.911	3.885	4.224
Mn1-O1	1.858	1.850	1.878	1.841	1.870	1.850	1.845
Mn1-O3	1.906	1.886	1.926	1.923	1.888	1.884	1.873
Mn1-O5	3.367	3.152	2.250	3.188	3.511	3.233	1.871
Mn2-O1	1.885	1.895	1.861	1.915	1.870	1.905	1.895
Mn2-O2	1.788	1.878	1.820	1.869	1.791	1.869	1.870
Mn2-O3	1.926	2.324	1.908	2.302	1.893	2.351	2.249
Mn3-O2	1.916	1.807	1.879	1.858	1.888	1.823	1.822
Mn3-O3	2.020	1.925	2.001	1.977	2.330	1.866	1.886
Mn3-O4	1.828	1.844	1.861	1.838	2.087	1.969	1.943
Mn3-O5	2.381	1.991	2.285	1.840	1.862	1.842	1.901
Mn4-O4	1.871	1.875	1.845	1.866	1.962	1.994	2.109
Mn4-O5	2.002	2.161	2.917	1.898	1.866	1.897	3.261
Mn4-W1	2.053	2.100	2.177	2.097	2.069	2.084	2.166
Mn4-W2	1.892	1.871	1.894	2.041	1.885	1.862	1.945
Ca-O1	2.518	2.489	2.459	2.501	2.514	2.485	2.475
Ca-O2	2.648	2.558	2.617	2.499	2.566	2.545	2.542
Ca-O5	2.494	2.613	2.491	2.673	2.542	2.654	2.763

	S_0H-4a S_2L-4a	S_0H-4b S_2L-4b	S_0H-5a S_2L-5a	S_0H-5b S_2L-5b	S_2L-6	S_2L-7
Mn1-Mn2	2.771	2.885	2.797	2.872	2.794	2.782
Mn1-Mn3	3.588	3.326	3.380	3.329	3.381	3.425
Mn1-Mn4	5.230	5.057	5.156	5.307	5.304	5.286
Mn2-Mn3	2.864	2.926	2.796	2.911	2.819	2.806
Mn2-Mn4	5.301	5.417	5.251	5.510	5.538	5.416
Mn3-Mn4	2.865	2.872	2.935	2.944	3.119	3.152
Mn1-Ca	3.769	3.703	3.761	3.714	3.773	3.824
Mn2-Ca	3.390	3.388	3.430	3.415	3.377	3.499
Mn3-Ca	3.549	3.500	3.695	3.539	3.827	3.827
Mn4-Ca	3.846	3.925	3.896	4.104	4.447	4.006
Mn1-O1	1.872	1.853	1.859	1.850	1.877	1.859
Mn1-O3	1.896	1.887	1.916	1.901	1.926	1.932
Mn1-O5	3.464	3.272	3.310	3.112	2.640	3.485
Mn2-O1	1.869	1.894	1.884	1.886	1.864	1.873
Mn2-O2	1.800	1.888	1.799	1.899	1.833	1.812
Mn2-O3	1.898	2.357	1.933	2.330	1.925	1.943
Mn3-O2	1.875	1.824	1.895	1.814	1.876	1.872
Mn3-O3	2.264	1.881	2.003	1.895	2.017	1.993
Mn3-O4	2.138	1.924	1.853	1.881	1.839	1.943
Mn3-O5	1.887	1.859	2.362	1.962	2.839	2.484
Mn4-O4	1.957	2.155	1.819	1.821	1.857	1.987
Mn4-O5	1.825	1.835	2.003	2.263	2.991	1.955
Mn4-W1	2.061	2.031	2.051	2.178	2.116	2.027
Mn4-W2	2.036	2.178	2.009	2.012	1.877	1.840
Ca-O1	2.498	2.486	2.513	2.513	2.474	2.548
Ca-O2	2.570	2.507	2.630	2.513	2.573	2.722
Ca-O5	2.567	2.669	2.493	2.608	3.089	2.540

	S_3L-1	S_3L-2	S_3L-3	S_3L-4	S_3L-5	S_3L-6	S_3L-7
Mn1-Mn2	2.803	2.794	2.907	2.781	2.784	2.754	2.776
Mn1-Mn3	3.447	3.382	3.408	3.174	3.669	3.039	3.750
Mn1-Mn4	5.224	5.322	5.266	5.384	5.433	5.620	5.406
Mn2-Mn3	2.849	2.806	2.928	2.812	2.912	2.864	2.938
Mn2-Mn4	5.270	5.391	5.413	5.579	5.455	5.682	5.443
Mn3-Mn4	2.803	3.143	2.878	3.278	2.921	3.240	2.904
Mn1-Ca	3.801	3.899	3.864	3.853	3.714	3.619	3.726
Mn2-Ca	3.389	3.476	3.338	3.549	3.398	3.455	3.404
Mn3-Ca	3.559	3.894	3.568	3.759	3.569	3.448	3.589
Mn4-Ca	3.918	4.088	4.041	4.050	4.040	4.153	4.028
Mn1-O1	1.891	1.863	1.849	1.860	1.877	1.875	1.876
Mn1-O3	1.932	1.927	1.842	2.031	1.896	1.897	1.892
Mn1-O5	3.355	1.778	3.391	2.098	3.646	1.752	3.638
Mn2-O1	1.856	1.863	1.914	1.854	1.847	1.849	1.845
Mn2-O2	1.827	1.797	1.844	1.828	1.800	1.831	1.799
Mn2-O3	1.917	1.903	2.366	1.872	1.889	1.876	1.881
Mn3-O2	1.882	1.900	1.835	1.896	1.865	1.858	1.866
Mn3-O3	2.041	2.050	1.979	2.015	2.379	2.164	2.456
Mn3-O4	1.802	1.823	1.828	1.799	2.096	2.040	2.078
Mn3-O5	1.841	3.047	1.923	1.885	1.887	2.079	1.883
Mn4-O4	1.934	1.875	1.917	1.913	1.960	2.000	1.962
Mn4-O5	1.926	3.935	1.964	3.344	1.877	3.959	1.872
Mn4-W1	2.023	2.009	2.006	2.021	2.062	2.001	2.045
Mn4-W2	1.882	1.906	1.874	1.902	1.875	1.875	1.877
Ca-O1	2.533	2.601	2.546	2.693	2.525	2.579	2.526
Ca-O2	2.548	2.655	2.525	2.569	2.584	2.527	2.607
Ca-O5	2.596	3.507	2.629	3.303	2.574	2.882	2.567

	S_1L-1	S_1L-2	S_1L-3a	S_1L-3b	S_1L-4	S_1L-5	S_1L-6	S_1L-7a	S_1L-7b
Mn1-Mn2	2.901	2.917	2.924	2.881	2.908	2.904	2.892	2.908	2.886
Mn1-Mn3	3.467	3.126	3.254	3.065	3.253	3.252	3.495	3.494	3.205
Mn1-Mn4	5.259	4.633	4.959	5.243	4.824	5.463	5.316	5.306	5.606
Mn2-Mn3	2.981	2.946	2.911	2.922	2.954	2.940	2.967	2.930	2.879
Mn2-Mn4	5.436	5.351	5.497	5.835	5.443	5.788	5.587	5.505	5.782
Mn3-Mn4	2.961	2.832	3.029	3.365	2.989	3.210	3.084	3.144	3.397
Mn1-Ca	3.782	3.485	3.630	3.374	3.634	3.615	3.698	3.825	3.664
Mn2-Ca	3.408	3.381	3.366	3.379	3.371	3.415	3.379	3.396	3.404
Mn3-Ca	3.658	3.432	3.441	3.568	3.464	3.520	3.749	3.736	3.573
Mn4-Ca	3.920	3.723	3.821	4.235	3.726	4.253	4.228	3.983	4.167
Mn1-O1	1.838	1.848	1.842	1.872	1.847	1.856	1.844	1.840	1.859
Mn1-O3	1.913	1.922	1.921	1.903	1.932	1.937	1.940	1.934	1.906
Mn1-O5	3.420	2.458	2.884	1.753	2.793	2.497	2.701	3.510	2.792
Mn2-O1	1.922	1.934	1.931	1.885	1.910	1.905	1.890	1.918	1.890
Mn2-O2	1.864	1.857	1.846	1.893	1.879	1.888	1.904	1.858	1.901
Mn2-O3	2.327	2.220	2.290	2.238	2.295	2.237	2.338	2.374	2.290
Mn3-O2	1.893	1.878	1.848	1.833	1.866	1.837	1.847	1.831	1.803
Mn3-O3	2.016	2.004	1.943	1.980	1.935	1.993	1.996	1.984	1.876
Mn3-O4	1.848	1.785	1.899	1.963	1.907	1.794	1.864	1.980	1.958
Mn3-O5	2.385	1.814	1.788	2.369	1.787	1.959	3.271	2.461	1.909
Mn4-O4	1.866	2.093	2.338	2.149	2.338	1.980	1.840	1.977	2.066
Mn4-O5	1.995	2.197	2.123	3.561	2.080	3.002	3.258	1.936	2.829
Mn4-W1	2.100	2.340	2.299	2.190	2.244	2.116	2.150	2.036	2.162
Mn4-W2	1.906	2.234	2.013	1.979	2.161	2.149	1.921	1.853	1.930
Ca-O1	2.525	2.454	2.469	2.427	2.473	2.509	2.483	2.503	2.487
Ca-O2	2.525	2.472	2.520	2.556	2.505	2.490	2.501	2.591	2.556
Ca-O5	2.504	2.568	2.557	2.598	2.571	2.563	2.610	2.543	2.593

	S_0L-1	S_0L-2	S_0L-3	S_0L-4	S_0L-5	S_0L-6
Mn1-Mn2	2.908	2.904	2.895	2.897	2.897	2.900
Mn1-Mn3	3.338	3.437	3.489	3.503	3.525	3.431
Mn1-Mn4	5.054	5.224	5.447	5.460	5.498	5.222
Mn2-Mn3	2.974	2.950	2.978	2.972	2.942	2.973
Mn2-Mn4	5.434	5.569	5.655	5.658	5.788	5.528
Mn3-Mn4	2.939	3.168	3.190	3.180	3.500	3.115
Mn1-Ca	3.598	3.731	3.685	3.710	3.709	3.769
Mn2-Ca	3.395	3.410	3.378	3.375	3.354	3.396
Mn3-Ca	3.565	3.658	3.775	3.729	3.843	3.627
Mn4-Ca	3.850	3.937	4.239	4.211	4.235	3.865
Mn1-O1	1.842	1.838	1.843	1.842	1.856	1.846
Mn1-O3	1.902	1.924	1.930	1.929	1.972	1.921
Mn1-O5	2.808	3.137	2.607	2.576	2.455	3.166
Mn2-O1	1.935	1.928	1.902	1.901	1.885	1.909
Mn2-O2	1.853	1.849	1.878	1.884	1.906	1.885
Mn2-O3	2.278	2.334	2.305	2.328	2.347	2.338
Mn3-O2	1.909	1.856	1.895	1.879	1.826	1.871
Mn3-O3	2.016	2.012	2.026	2.019	1.987	1.989
Mn3-O4	1.821	1.933	1.815	1.826	1.953	1.944
Mn3-O5	2.270	2.308	3.272	3.282	3.056	2.256
Mn4-O4	2.017	2.223	1.979	1.960	2.069	2.225
Mn4-O5	2.340	2.175	3.446	3.495	3.297	2.132
Mn4-W1	2.277	2.284	2.148	2.111	2.161	2.202
Mn4-W2	2.256	2.019	2.058	2.223	1.920	2.162
Ca-O1	2.479	2.493	2.503	2.512	2.469	2.511
Ca-O2	2.502	2.613	2.487	2.463	2.535	2.551
Ca-O5	2.445	2.459	2.592	2.617	2.814	2.466

Part V. Mulliken spin populations for the Mn ions of the inorganic core

	Mn1	Mn2	Mn3	Mn4
S_2H-1a	3.88	2.92	2.85	2.87
S_2H-1b	2.89	2.83	2.84	3.84
S_2H-2a	3.88	2.92	2.87	2.89
S_2H-2b	2.89	2.83	2.86	3.86
S_2H-3	3.86	2.92	2.85	2.87
S_3H-1	2.84	2.89	2.85	2.87
S_3H-2	2.85	2.89	2.84	2.88
S_3H-3	2.88	2.83	2.79	2.86
S_3H-4	2.87	2.84	2.84	2.83
S_3H-5	2.88	2.84	2.87	2.78
S_1H-1a	3.73	2.78	2.75	3.74
S_1H-1b	3.87	3.87	2.89	2.86
S_1H-2	3.89	2.89	2.88	3.90
S_1H-3a	3.92	2.89	2.92	3.84
S_1H-3b	3.90	2.91	2.89	3.85
S_0H-1a / S_2L-1a	3.87	2.89	3.86	3.90
S_0H-1b / S_2L-1b	3.86	3.86	2.91	3.88
S_0H-1c / S_2L-1c	3.73	2.81	3.70	3.76
S_0H-2 / S_2L-2	3.90	3.86	2.92	3.88
S_0H-3a / S_2L-3a	3.90	2.91	3.85	3.87
S_0H-3b / S_2L-3b	3.88	3.87	2.90	3.86
S_0H-3c / S_2L-3c	2.96	3.82	2.97	4.73
S_0H-4a / S_2L-4a	3.90	2.91	3.87	3.88
S_0H-4b / S_2L-4b	3.89	3.86	2.93	3.91
S_0H-5a / S_2L-5a	3.88	2.91	3.85	3.91
S_0H-5b / S_2L-5b	3.87	3.86	2.93	3.89
S_2L-6	3.90	2.94	3.83	3.88
S_2L-7	3.86	2.92	3.91	3.89
S_3L-1	3.91	2.92	2.86	3.87
S_3L-2	2.84	2.89	3.86	3.91
S_3L-3	2.90	3.82	2.92	3.88
S_3L-4	3.81	2.89	2.94	3.90
S_3L-5	2.86	2.89	3.86	3.87
S_3L-6	2.80	2.88	3.92	3.88
S_3L-7	2.86	2.89	3.87	3.87
S_3L-8	3.91	2.91	2.89	3.88
S_3L-9	3.87	2.93	3.85	2.91
S_3L-10	2.92	2.89	3.83	3.91
S_3L-11	3.91	2.92	2.90	3.86
S_3L-12	2.98	2.88	3.85	3.90
S_1L-1	3.89	3.88	3.88	3.90
S_1L-2	3.93	3.86	2.80	4.83
S_1L-3a	3.92	3.85	2.88	4.81
S_1L-3b	2.77	3.86	3.90	4.84

S_1L-4	3.93	3.85	2.90	4.84
S_1L-5	3.92	3.86	2.95	4.79
S_1L-6	3.91	3.88	3.83	3.90
S_1L-7a	3.90	3.86	3.91	3.91
S_1L-7b	3.91	3.87	2.96	4.79
S_0L-1	3.93	3.88	3.87	4.82
S_0L-2	3.90	3.87	3.92	4.84
S_0L-3	3.92	3.89	3.92	4.77
S_0L-4	3.91	3.89	3.91	4.80
S_0L-5	3.94	3.88	3.91	4.82
S_0L-6	3.92	3.87	3.92	4.86

Part VI. Q-band ^{55}Mn-Davies ENDOR at 2.5 K of the S_2 state of the Mn_4O_5Ca cofactor isolated from *T. elongatus*

Test measurements for a mixed valence $Mn^{II}Mn^{III}$ model complex with fast T_1 relaxation: Test measurements were performed on a bis-μ-pivalato-μ-hydroxo $Mn^{II}Mn^{III}$ model complex (PivOH),[21] see Fig. 4B. It displays ^{55}Mn-ENDOR resonances across a large spectral range (100–400 MHz), making it an ideal system to check ENDOR performance of the instrument. The spectra measured for the PivOH complex are essentially the same as reported in Cox et al.,[22] measured at 5 K using an Oxford Helium flow cryostat system. Using the new cryogenic closed cycle cryostat system, it was found that the optimal temperature for the ^{55}Mn-ENDOR measurement was approximately 3.5 K. At this temperature the electronic T_1 relaxation ($T_1^* = 35$ μs, $T_1 = 46$ μs Fig. S13B) is sufficiently slow that a near full inversion of the spin echo is maintained during the Davies pulse sequence (ca. 6 μs), but is sufficiently fast to allow efficient data collection, with repetition rates of the order of one ms. Below this temperature (2.5 K) the ENDOR performance drops owing to a dramatic increase in the T_1 time ($T_1^* = 610$ μs, $T_1 = 820$ μs), slowing the maximum rate of data collection, limiting the number of averages that can be collected in a reasonable time frame (10–20 hours). Importantly, no change was observed for the ^{55}Mn-ENDOR signal envelope although the electronic T_1 time increased by twentyfold. It is noted that electronic T_2 relaxation is approximately temperature invariant (twofold slower) as expected (Fig. S13A). A second, faster phase seen in T_1^* decay curves (25-36%) is assigned to sample aggregation. It is also noted that T_1 times as estimated by inversion recovery are similar (within a factor of two), suggesting spectral diffusion does not need to be explicitly considered in this system.[23]

Calibration of B_2 (RF) field using the PivOH complex: The B_2 (RF) field was calibrated at a series of RF frequencies through the ^{55}Mn-ENDOR signal envelope, see Fig. 4A and 4B. The optimal RF π pulse (t_{RF}) was estimated by performing an RF nutation experiment at a series of positions through the profile marked in Fig. 4B. Here the ENDOR response is

monitored as a function of the length of the t_{RF} pulse using the Davies pulse sequence: t_{inv}–t_{RF}–T–t_p–t–$2t_p$–t–echo. To eliminate a heating artifact, a background nutation curve measured at position where no ^{55}Mn-ENDOR resonances appear (185 MHz) was subtracted from the data. It is readily seen that the optimal RF π pulse (t_{RF}) was found to be ca. 4 μs at all positions and that no suppression of high frequency transitions (> 200 MHz) is observed. As hyperfine enhancement does not need to be considered in this system, these results require that the B_2 field is linear over the 100–300 MHz range. Above 300 MHz, the B_2 field does begin to fall off, but NMR resonances can still be observed.

^{55}Mn-ENDOR and T_1 decay of the S_2 (multiline) state of the Mn_4O_5Ca cofactor at 2.5 K: ^{55}Mn-ENDOR spectra were collected for the Mn_4O_5Ca cofactor poised in the S_2 state at the center field of the multiline signal (Fig. 4C, insert). As mentioned in the main text, the electronic T_1 relaxation (T_1^* = 21 μs, T_1 = 41 μs) at 5 K is fast enough to allow efficient data collection with repetition rates of the order of 1 ms while slow enough that a near full inversion of the spin echo is maintained during the Davies pulse sequence (≈6 μs), see Fig. S13D. Figure 4C shows that the ^{55}Mn-ENDOR signals are only observed over a narrow radio frequency range, in line with a tetramer spin projection model.[24-27]

^{55}Mn-ENDOR spectra were also collected at 2.5 K, Fig. 4C. Although data collection is more difficult with a T_1 time of at least ca. 2 ms at this temperature, ^{55}Mn-ENDOR data at a comparable signal to noise ratio could be obtained. As expected, the ENDOR spectrum is essentially identical to that seen at 5 K.

It should be pointed out that here we report only an upper bound estimate for the electronic T_1 of the multiline signal at 2.5 K, since spectral diffusion significantly contributes to the longitudinal (effective T_1) relaxation at 2.5 K. This can be readily seen by comparing the inversion recovery and simulated decay traces. For the inversion recovery decay, the major species decays with a time constant of T_1 = 27 ms (37 s^{-1}), whereas for the simulated three-pulse 2.5 K data the decay of the major species is an order of magnitude faster (T_1^* = 1.7 ms,

590 s^{-1}) as this measurement is more susceptible to spectral diffusion. Importantly though, the electronic T_1 estimate as inferred from the simulated decay trace ***must*** represent an underestimation of the T_1 relaxation rate of the multiline signal and thus is a robust upper bound estimate for it electronic T_1 relaxation.[23] The real value should be closer to the inversion recovery decay estimate i.e. T_1 = 27 ms (37 s^{-1}).

Finally, it should also be noted that in both 2.5 K decay traces there is a very fast component not included in the bi-exponential fit. This component decayed completely within 300 µs and is tentatively assigned to an underlying contribution from the semiquinone-iron signal ($Q^{\bullet-}Fe^{2+}$).

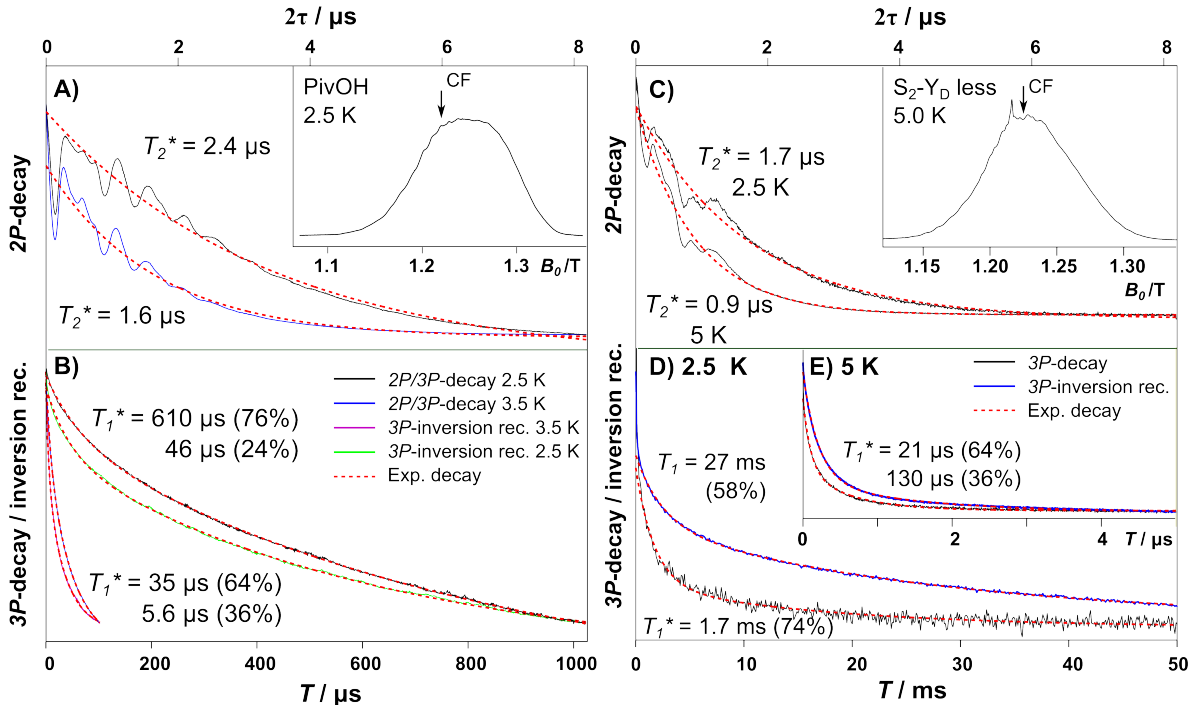

Figure S13. Q-band pulse EPR of the PivOH complex and S_2 state at center field (see insert). **A**) The decay of the PivOH signal, measured using a two pulse sequence as a function of the interpulse separation τ. **B**) The decay of the PivOH signal, measured using a three pulse sequence as a function of the interpulse separation T. **C**) The decay of the multiline signal at 2.5 K, measured using a two pulse sequence as a function of the interpulse separation τ. **D), E)** The decay of the multiline signal measured using a three pulse sequence as a function of the interpulse separation T. For details see the materials and methods section in the main text.

Part VII. Additional analysis of calculated Mn K pre-edge X-ray absorption spectra

A metal K pre-edge spectrum gains intensity through p-d-mixing, therefore distortion from the ideal octahedral symmetry for hexacoordinate metal centers enhances the intensity of the transition. The most intense transitions contributing to the first peak of the calculated spectra are those into the unoccupied molecular orbitals with predominant Mn 3d character, e.g. the local α e_g-type orbitals for octahedrally coordinated Mn(IV) ions with a $3d^3$ configuration. For Mn(II), Mn(III) and Mn(IV) with local $3d^5$, $3d^4$ and $3d^3$ configurations, respectively, there are five (into five unoccupied β orbitals), six (into one unoccupied α and five unoccupied β orbitals) and seven (into two unoccupied α and five unoccupied β orbitals) transitions. The total calculated spectra as shown in the main text, Figure 9, are the sums of the spectra from the individual Mn ions. Deconvolutions into individual contributions are shown and discussed in the following.

From Figure S15 it can be seen that the calculated Mn(II) and Mn(III) spectra start at lower energies than those of Mn(IV) (Mn2 in **S_2L-6**, Mn2 and Mn3 in **S_3L-3**), which explains why the maxima in the spectra of the S_0L and S_1L models appear at lower energies than those in the spectra of the S_2L and S_3L models: the spectra of S_0L and S_1L arise exclusively from Mn(II) and Mn(III) contributions at low energies, whereas for S_2L and S_3L the higher energy contributions of the Mn(IV) ions shift the maximum of the total spectrum to higher energy.

The intensity differences arise from differences in the local Mn geometries. For example, it is often observed that square pyramidally coordinated metal centers show higher pre-edge intensities than octahedrally coordinated centers.[28] This explains the intensity difference between the spectra of **S_0L-3**, where O5 is a loosely coordinated H_2O molecule, and **S_1L-1**, where all Mn ions except Mn1 are hexacoordinate.

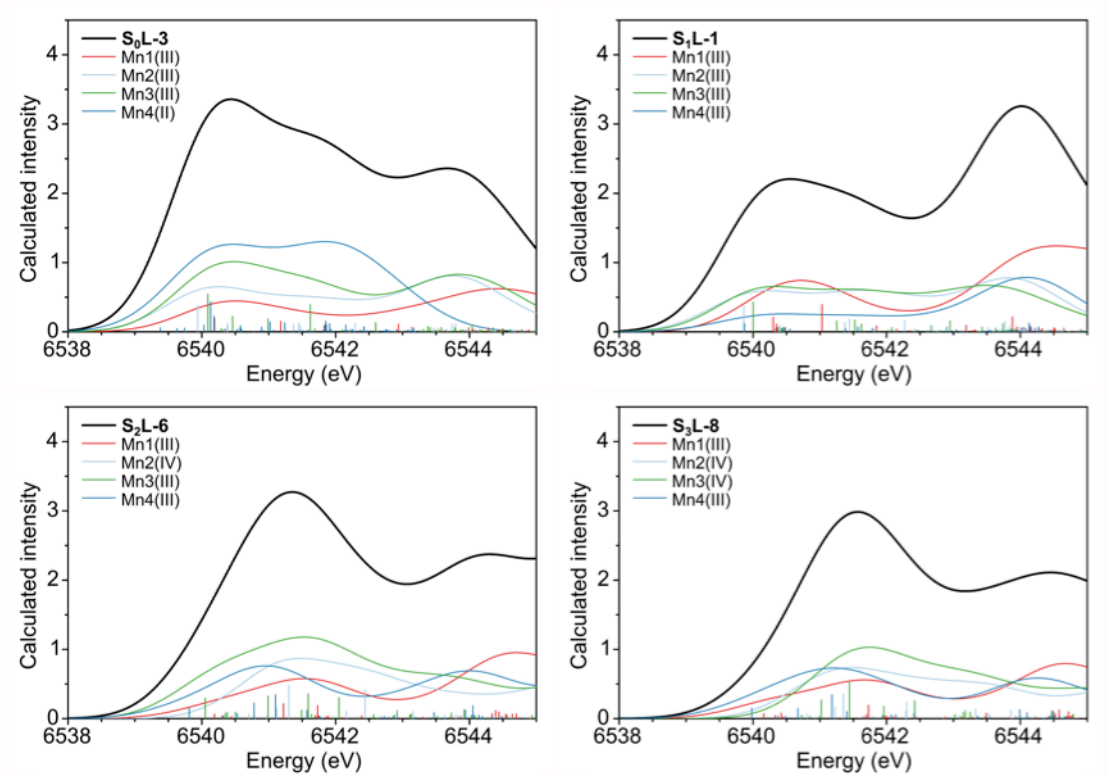

Figure S14. Spectra of selected low-valent models with their contributions from the individual Mn ions.

Due to the higher structural consistency within the sequence of models that belong to the high-valent scheme, it is easier to relate spectral changes to changes in electronic and geometric structure. Comparing the development of the individual Mn contributions as the cluster advances in the Kok cycle (Figure S16), it can be seen that the contribution of each Mn center to the total spectrum evolves as expected in each S state transition. For example, the contribution of Mn2, which is present as an octahedrally coordinated Mn(IV) ion in all high-valent S state models (light blue trace in Figure S16), undergoes only minor changes, whereas the oxidation of Mn3 from Mn(III) to Mn(IV) in the S_0 to S_1 transition induces an increase in intensity for its spectral contribution to the total spectrum (green trace).

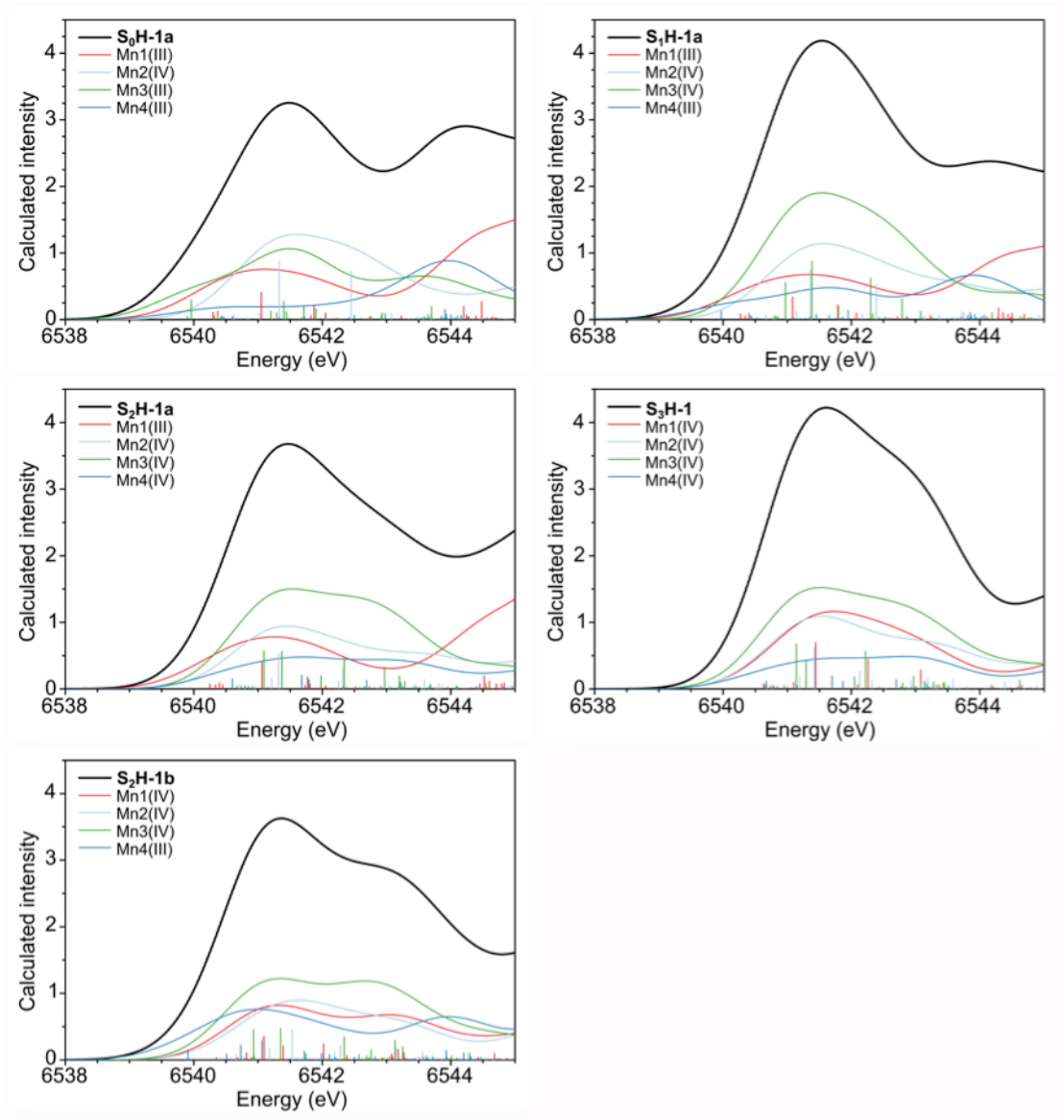

Figure S15. Spectra of selected high-valent models with their contributions from the individual Mn ions.

Part VIII. Analysis of low-valent models in terms of super-reduced S states

The LV structures reported in this work may serve as models of super-reduced (negative) S states of the OEC. Specifically, the S_1L and S_0L models presented in this work are candidates for the S_{-1} and S_{-2} states of the OEC, respectively. Such negative states have been invoked to rationalize the photoreduced crystallographic model of PSII, but they are also accessible by chemical[29, 30] and other[31] treatments and have been studied experimentally by XANES,[32] EXAFS,[29] and EPR spectroscopies.[30, 33-36] Importantly, the structural integrity of the Mn_4Ca cluster seems to be maintained in the negative S states as they can be flash-advanced to active, O_2-evolving centers.[33, 37] The protonation level of reduced states with respect to S_0 is ill-defined, but based on the relative energies and whether the models can be formally connected to **S_0H-1**, potential candidates for S_{-1} (**S_1L-1**, **S_1L-6**, and **S_1L-7a**) and S_{-2} (**S_0L-3**, **S_0L-4**, and **S_0L-6**) can be identified among the models presented in this paper (see Figure S16).

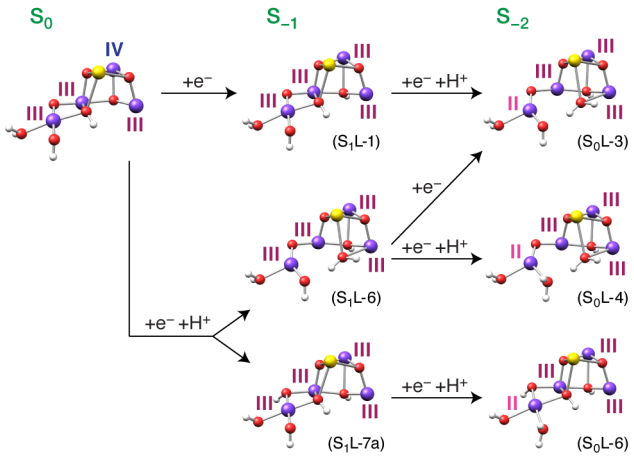

Figure S16. Possible pathways for the formation of reduced S_{-1} and S_{-2} states. The labels in parentheses refer to the corresponding LV models reported in this study.

Geometries of OEC models with average oxidation states lower than those for S_0 have been compared to the crystal structure of 1.9 Å resolution to assess the extent of radiation damage.[38] According to this study, the inorganic core of the crystal structure can be structurally reproduced best by a mixture of S_{-4} (2%), S_{-3} (56%), S_{-2} (16%), S_{-1} (12%) and S_0

(14%) models. One of the S_{-1} models best matching the crystal structure in that study has the same protonation pattern as model **S_1L-7a**, and the best S_{-2} model has the same protonation pattern as **S_0L-6**. If **S_0L-6** corresponds to the physiological S_{-2} state, model **S_0H-1** could be reached with single proton losses at each oxidation step, thus connecting the super-reduced models (Figure S16) to the catalytic cycle. A Mn(II)-Mn(III) dimer was proposed to exist for states reduced below S_{-1},[33-35, 37] which agrees well with the candidates identified above, where all plausible S_{-1} models have a $Mn(III)_4$ and all S_{-2} models a $Mn(II)Mn(III)_3$ configuration. All these models are characterized by high spin ground states ($S_{GS} \geq 3$ for S_{-1} and $S_{GS} \geq 7/2$ for S_{-2}). Although S_{-1} and S_{-2} have been proposed to possess low-spin coupled Mn clusters leading to a diamagnetic $S_{GS} = 0$ ground state for S_{-1} and an $S_{GS} = 1/2$ state for S_{-2},[37, 39] such low spin intermediate states are only EPR-visible upon addition of NO, a paramagnetic molecule itself, making direct comparison of spin states impossible at this time. We also cannot exclude that the structure of the cluster is significantly perturbed by the reductants used in chemical treatments of the S_0 state, or that over-reduction *per se* leads to conformational changes that are not covered by the present models.

References

1. Y. Umena, K. Kawakami, J.-R. Shen and N. Kamiya, *Nature*, 2011, **473**, 55-60.
2. D. A. Pantazis, M. Orio, T. Petrenko, S. Zein, E. Bill, W. Lubitz, J. Messinger and F. Neese, *Chem.—Eur. J.*, 2009, **15**, 5108-5123.
3. D. A. Pantazis, M. Orio, T. Petrenko, S. Zein, W. Lubitz, J. Messinger and F. Neese, *Phys. Chem. Chem. Phys.*, 2009, **11**, 6788-6798.
4. M. Orio, D. A. Pantazis and F. Neese, *Photosynth. Res.*, 2009, **102**, 443-453.
5. V. Krewald, F. Neese and D. A. Pantazis, *J. Am. Chem. Soc.*, 2013, **135**, 5726-5739.
6. M. Orio, D. A. Pantazis, T. Petrenko and F. Neese, *Inorg. Chem.*, 2009, **48**, 7251-7260.
7. S. Schinzel and M. Kaupp, *Can. J. Chem.*, 2009, **87**, 1521-1539.
8. D. A. Pantazis, V. Krewald, M. Orio and F. Neese, *Dalton Trans.*, 2010, **39**, 4959-4967.
9. J. Schraut, A. V. Arbuznikov, S. Schinzel and M. Kaupp, *ChemPhysChem*, 2011, **12**, 3170-3179.
10. D. Bovi and L. Guidoni, *J. Chem. Phys.*, 2012, **137**, 114107.
11. C. Baffert, M. Orio, D. A. Pantazis, C. Duboc, A. G. Blackman, G. Blondin, F. Neese, A. Deronzier and M.-N. Collomb, *Inorg. Chem.*, 2009, **48**, 10281-10288.
12. C.-L. Zhou, Z.-M. Wang, B.-W. Wang and S. Gao, *Dalton Trans.*, 2012, **41**, 13620-13625.
13. T. C. Stamatatos, D. Foguet-Albiol, S.-C. Lee, C. C. Stoumpos, C. P. Raptopoulou, A. Terzis, W. Wernsdorfer, S. O. Hill, S. P. Perlepes and G. Christou, *J. Am. Chem. Soc.*, 2007, **129**, 9484-9499.
14. J. S. Kanady, E. Y. Tsui, M. W. Day and T. Agapie, *Science*, 2011, **333**, 733-736.
15. S. Mukherjee, J. A. Stull, J. Yano, T. C. Stamatatos, K. Pringouri, T. A. Stich, K. A. Abboud, R. D. Britt, V. K. Yachandra and G. Christou, *Proc. Natl. Acad. Sci. U.S.A.*, 2012, **109**, 2257-2262.
16. C. Philouze, G. Blondin, J.-J. Girerd, J. Guilhem, C. Pascard and D. Lexa, *J. Am. Chem. Soc.*, 1994, **116**, 8557-8565.
17. G. Blondin, R. Davydov, C. Philouze, M.-F. Charlot, S. Styring, B. Åkermark, J.-J. Girerd and A. Boussac, *J. Chem. Soc., Dalton Trans.*, 1997, 4069-4074.
18. G. Karotsis, L. F. Jones, G. S. Papaefstathiou, A. Collins, S. Parsons, T. D. Nguyen, M. Evangelisti and E. K. Brechin, *Dalton Trans.*, 2008, 4917-4925.
19. C. E. Dubé, S. Mukhopadhyay, P. J. Bonitatebus, R. J. Staples and W. H. Armstrong, *Inorg. Chem.*, 2005, **44**, 5161-5175.
20. J.-Z. Wu, E. Sellitto, G. P. A. Yap, J. Sheats and G. C. Dismukes, *Inorg. Chem.*, 2004, **43**, 5795-5797.
21. U. Bossek, H. Hummel, T. Weyhermüller, K. Wieghardt, S. Russell, L. van der Wolf and U. Kolb, *Angew. Chem., Int. Ed.*, 1996, **35**, 1552-1554.
22. N. Cox, W. Ames, B. Epel, L. V. Kulik, L. Rapatskiy, F. Neese, J. Messinger, K. Wieghardt and W. Lubitz, *Inorg. Chem.*, 2011, **50**, 8238-8251.
23. A. Schweiger and G. Jeschke, *Principles of pulse electron paramagnetic resonance*, Oxford University Press, Oxford, 2001.
24. L. V. Kulik, B. Epel, W. Lubitz and J. Messinger, *J. Am. Chem. Soc.*, 2005, **127**, 2392-2393.
25. L. V. Kulik, B. Epel, W. Lubitz and J. Messinger, *J. Am. Chem. Soc.*, 2007, **129**, 13421-13435.
26. J. M. Peloquin, K. A. Campbell, D. W. Randall, M. A. Evanchik, V. L. Pecoraro, W. H. Armstrong and R. D. Britt, *J. Am. Chem. Soc.*, 2000, **122**, 10926-10942.
27. J. M. Peloquin and R. D. Britt, *Biochim. Biophys. Acta Bioenerg.*, 2001, **1503**, 96-111.

28. T. E. Westre, P. Kennepohl, J. G. DeWitt, B. Hedman, K. O. Hodgson and E. I. Solomon, *J. Am. Chem. Soc.*, 1997, **119**, 6297-6314.
29. P. J. Riggs-Gelasco, R. Mei, C. F. Yocum and J. E. Penner-Hahn, *J. Am. Chem. Soc.*, 1996, **118**, 2387-2399.
30. C. Goussias, N. Ioannidis and V. Petrouleas, *Biochemistry*, 1997, **36**, 9261-9266.
31. M. Higuchi, T. Noguchi and K. Sonoike, *Biochim. Biophys. Acta Bioenerg.*, 2003, **1604**, 151-158.
32. P. J. Riggs, C. F. Yocum, J. E. Penner-Hahn and R. Mei, *J. Am. Chem. Soc.*, 1992, **114**, 10650-10651.
33. N. Ioannidis, J. Sarrou, G. Schansker and V. Petrouleas, *Biochemistry*, 1998, **37**, 16445-16451.
34. J. Sarrou, N. Ioannidis, Y. Deligiannakis and V. Petrouleas, *Biochemistry*, 1998, **37**, 3581-3587.
35. J. Hanley, J. Sarrou and V. Petrouleas, *Biochemistry*, 2000, **39**, 15441-15445.
36. J. Sarrou, S. Isgandarova, J. Kern, A. Zouni, G. Renger, W. Lubitz and J. Messinger, *Biochemistry*, 2003, **42**, 1016-1023.
37. G. Schansker, C. Goussias, V. Petrouleas and A. W. Rutherford, *Biochemistry*, 2002, **41**, 3057-3064.
38. A. Galstyan, A. Robertazzi and E. W. Knapp, *J. Am. Chem. Soc.*, 2012, **134**, 7442-7449.
39. D. Koulougliotis, *Photosynthetica*, 2009, **47**, 567-574.